

Evaporation-based, co-axial lock-and-key fibrous reservoir for long-term prevention of hypertrophic scars

Ho-Pan Beia, Tianpeng Xua, Jing Zhou, Zhifei Donga, Yufeng Wangc, Kak-Yuen Wongd, Huaiyu Wange, Xin Zhaoa,*

Abstract

Many diseases and conditions such as hypertrophic scarring require long-term maintenance over the healing cycle to achieve full recovery. However, there is a lack of wound dressings that can sustain over 90 days of therapeutic release. Inspired by the enhancement of wound healing by the nanofibrous morphology and diverse structures of electrospinning, we report an evaporation-based co-axial electrospun fibrous scaffold incorporating polymer brush gatekept nanocarriers for sustained delivery of therapeutics. The release rates of the system were demonstrated to be tunable through polymer graft length, while the system experienced minimal burst release when submerged under aqueous conditions. As a proof-of-concept, we target hypertrophic scarring by loading the system with doxorubicin, which led to inhibition of fibroblast activity without interfering with cell adhesion. Application of our scaffolds on rabbit ear hypertrophic scar models displayed that our scaffolds effectively reduced collagen density and scar-related gene expression in healing tissues, with improved tissue elevation outcomes. We envision that our long-term release scaffolds will be useful in combating long unresolved clinical dilemma such as tendon adhesion and tumor regression.

Keywords

Drug delivery, Electrospinning, Gatekeeper nanoparticles, Hypertrophic scarring, Long-term release

1. Introduction

Hypertrophic scarring is among the most common skin blemishes encountered by individuals throughout their lifetime. Any lacerating injuries, burns or skin conditions damaging the dermal layer will lead to incidence of scarring (40–70% post-surgery, 91% post-burn injury) [1]. The rapid and abnormal deposition of collagen that forms the scar tissues stem from the over-activity of fibroblasts near the trauma site [2]. While there are studies reporting the prevention of hypertrophic scars through anti-inflammatory or bio-based biomaterials, their anti-scarring efficiency leaves much to be desired as they are unable to inhibit the hyperactivity of fibroblasts during the late skin remodeling process after wound closure, despite evidence of accelerated healing [3,4]. Additionally, strategies such as sutures or tissue patches have low drug encapsulation potential or low diffusion distances, causing the therapeutic reservoir to deplete quickly without supporting the entire wound healing cycle [5].

To combat the growing scar tissues, the clinical gold standard involves the biweekly injection of anti-scarring agents (e.g., chemotherapy drugs, steroids, siRNAs) into the scar tissues [6]. However, that alone could not upkeep effective therapeutic window, as drug molecules quickly diffuse to the surrounding tissues, greatly lowering their localized concentration. Thus, combination of drug encapsulated wound dressings have emerged to achieve sustained release of anti-scarring agents to lengthen the therapeutic window before re-application. Amongst them, electrospun fibrous scaffolds have emerged as the most researched option for wound healing owing to their extracellular matrix (ECM)-mimetic structure, simple set up, and wide variety of material choices [7–10]. Notably, their nanofibrous structure promotes cell adhesion and water vapor transmission rate for dissipating exudate, while serving as a reliable physical barrier against pathogens. Numerous advanced electrospun fiber structures are employed nowadays with very limited success to lengthen the drug release profile including core-shell designs, incorporation of nanoparticles, and emulsion electrospinning [11–14]. Most notably, nanoparticles are exposed to harsh organic solvents during the

spinning process, greatly lowering their drug retention efficiency. Thus far, none of the studies are able to achieve over 90-day release profile (approximate to the complete wound healing cycle) due to the low diffusion distance and quick degradation of simple mesh networks. This is suboptimal for a wound dressing as its re-application potentially damages healing tissues, while the inability to upkeep local anti-scarring agent concentration during later remodeling stages of wound healing limits their capacity to prevent scar formation.

Herein, we propose a long-term drug releasing electrospun fibrous scaffold with core-shell design, imbued with gatekeeping nanoparticles as condensed drug reservoirs to achieve the much- desired >90 day release profile corresponding to typical wound healing cycle (Fig. 1). Mesoporous silica nanoparticles (MSNs) were chosen in this study for their FDA-approved safety and high drug encapsulation efficiency [15–17]. Through grafting hydrophobic poly lactic acid (PLA) brushes onto the surfaces of nanoparticles, the drug leakage in aqueous environments can be greatly reduced through the gatekeeping of pores. Drug loading is performed through mixing anti-scarring agents in mild organic solvents, which extends the PLA brushes to allow drug entry, while the gatekeepers' drug retention potential is fine-tuned through modulating the brush length by addition polymerization duration. For thorough dispersal of nanoparticles within the center of the electrospun fibers, pseudo-emulsion co-axial electrospinning was employed by encapsulating functionalized nanoparticles in ethanol as core and PLA as shell to form consistent nanofibers with reduced exposure of nanoparticles. During the electrospinning process, the staggered rates of spinning solvent and ethanol evaporation left the co-axial structure with simple FDA approved elements without compromising the lumen integrity. At the same time, the now dried lumen is shielded by hydrophobic PLA fiber shell to greatly slow down water influx, extending the drug release profile.

We found that the formed fibers demonstrated distinct, stable morphologies and sustained release of model drug doxorubicin (DOX) over 90 days. They also demonstrated anti-scarring efficacy when introduced to both in vitro human fibroblasts and rabbit ear hypertrophic scar models, with minimal impedance to wound healing but greatly reduced collagen deposition and expression of scar-related genes. The non-rigorous requirements and simple mechanism of our long-term drug releasing electrospun fibrous scaffold is expected to possess high adaptability and translation into clinical application and solve other tissue engineering dilemmas. Notably, this highly effective lock-and-key concept for long-term release can also be applied to various tissue scaffolds including inhibition of cancer development, tendon adhesion, as well as design of blood contacting coatings.

2. Materials and methods

2.1. Functionalization of MSN-PLAs with the graft-from approach

Carboxylic acid-functionalized MSNs (200 nm diameter, 4 nm pore size) were purchased from Sigma-Aldrich, and added to L-lactide as monomers and Tin(II) 2 ethylhexanoate as catalyst for ring-opening polymerization [18]. After purging the flask with nitrogen, the mixture was allowed to react under heating at 120 °C for 1, 3, 6, 24, and 48 h. After quenching the reaction with excess chloroform, the resultant powder was washed thrice with chloroform until no trace lactide or PLA can be detected in the supernatant. After air drying at 60 °C overnight, the nanoparticles were denoted MSN-PLA.

2.2. Characterization of MSN-PLAs

Transmission electron microscope (TEM) (Jeol JEM-2100F) was performed to assess the morphology of MSNs. To assess the are able to achieve over 90-day release profile (approximate to the complete wound

healing cycle) due to the low diffusion distance and quick degradation of simple mesh networks. This is suboptimal for a wound dressing as its reapplication potentially damages healing tissues, while the inability to upkeep local anti-scarring agent concentration during later remodelling stages of wound healing limits their capacity to prevent scar formation.

2.3. Loading of MSN-PLAs with doxorubicin

50 mg/mL DOX was dissolved in hexafluoro-2-propanol (HFIP) and stirred with MSN-PLAs overnight for drug loading. The loaded MSN-PLA-DOXs were then washed thrice with deionized water until supernatant becomes clear and collected using centrifugation. For drug release assessment, MSN-PLA-DOXs were dispersed in PBS, of which half is replaced at predetermined intervals and its DOX concentration was quantified with visible light- spectrometry at absorbance 480 nm. The cumulative drug release percentage was calculated at Cumulative release = volume of buffer (mL) \times drug concentration at time point t + \sum (volume removed \times concentration from previous time points) and cumulative percentage = drug released/drug loaded \times 100%.

2.4. Electrospinning of ethanol/MSN-PLA core-shell fibers

Ethanol/MSN-PLA core-shell fibers were fabricated via co-axial electrospinning. Co-axial spinning was employed with ethanol as the core solution to avoid direct mixing of nanoparticles with shell solution (PLA in HFIP) to prevent the leakage of DOX into the surroundings due to the open-up of PLA brushes in HFIP (Fig. S1). Briefly, 10, 20, or 50 mg of MSN-PLA-DOX were well dispersed in pure ethanol with ultrasound sonication for 30 min as core solution, and 10 kDa PLA was dissolved in HFIP (30% w/v) to serve as shell solution. Two 10 mL syringes were separately loaded with the respective solutions and connected to a co-axial needle (inner diameter: 0.9 mm, outer diameter: 1.8 mm). 17 kV voltage was supplied to the needle tip while -2 kV was supplied to the collector 10 cm away. The solutions were fed at 1:3 ratios for core-shell electrospinning. The spinning process was performed at room temperature and humidity for 1 h before the formed membranes were peeled off and air dried for further study.

2.5. Characterization of electrospun fibrous scaffolds

The morphology of ethanol/MSN-PLA core-shell fibers was assessed via TEM and scanning electron microscope (SEM) imaging. The average fiber diameter was measured using ImageJ on 5 different images per group obtained from TEM. The drug release profile was performed similarly to MSN-PLAs. Briefly, 1 cm diameter circles were cut from the scaffolds using a hole punch, and transferred to soaking in 1 mL PBS. At predetermined intervals, all of the supernatant was replaced and quantified in terms of DOX concentration with visible light-spectrometry at 470 nm excitation, 595 nm emission (Thermo Scientific Varioskan LUX Multimode Microplate Reader).

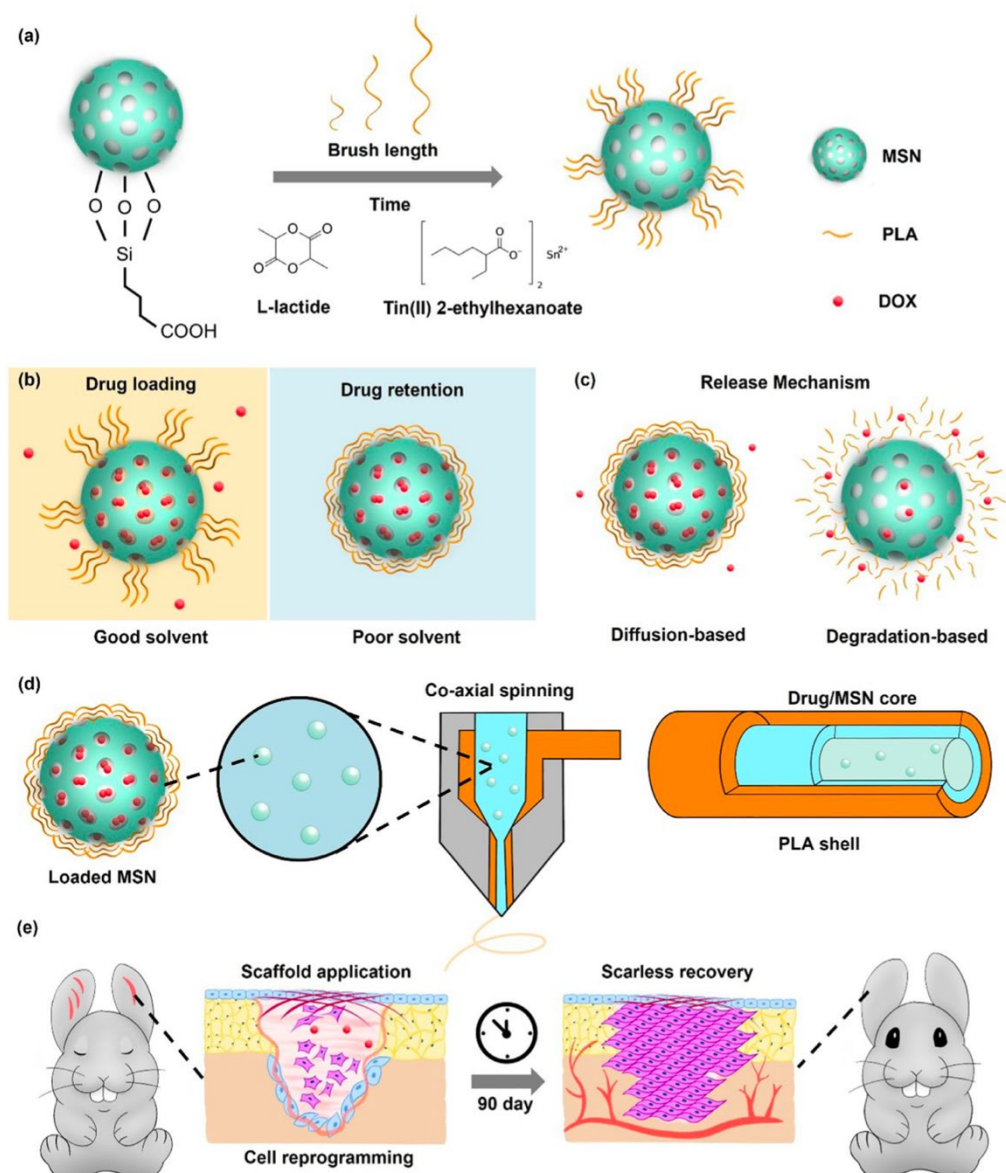


Fig. 1. Schematic depicting design, synthesis and application of the long-term drug releasing electrospun fibrous scaffold. (a) Grafting of polymer brush gatekeepers onto the surface of nanocarriers. (b) The “unlocked” and “locked” state of nanocarriers under good and poor solvent, respectively. (c) Release mechanism of the nanocarriers. (d) Co-axial spinning of core and shell solutions to form fibrous scaffolds. (e) Application of long-term drug releasing electrospun fibrous scaffolds as wound dressing for prevention of hypertrophic scarring.

2.6. *In vitro* biocompatibility, proliferation and adhesion study

Human fibroblasts (3T3s) were cultured in Dulbecco’s modified Eagle’s medium alpha containing 10% fetal bovine serum at 37 °C in a humidified atmosphere of 5% carbon dioxide. 3T3s were passaged at 70–80% confluency with Trypsin/EDTA, and before seeding onto scaffolds for further study. All studies were performed using cells at passage 6 or below. For toxicity assessment of nanoparticles, MSN-PLA-DOX was first soaked for 24 h in culture medium to release DOX. For quantification of different DOX concentrations, the medium was diluted by 1x, 10x, 100x, and 1000x and transferred to 96 well plates pre-seeded with 2000 cells. After 24 and 48 h, CCK-8 assay (Biosharp Life Sciences Cell Counting Kit-8) was used to determine proliferation of fibroblasts according to manufacturer’s instructions. For biocompatibility assessment of electrospun scaffolds, 2000 cells were each seeded in 96 well plate and then cultured using scaffold co-cultured medium for 24 h. CCK- 8 assay was used to determine proliferation of fibroblasts according to

manufacturer's instructions. For adhesion assessment, 1 cm circular membranes were cut from scaffolds using a hole punch and placed within a 48 well plate. Then, 5000 3T3 fibroblasts were seeded onto the top of the membranes and allowed to culture for 24 h. The cells were then fixed with 4% paraformaldehyde, permeated with Triton X-100, blocked with buffer solution and stained using 594 phalloidin and 4',6-diamidino-2-phenylindole (DAPI) for observation of actin and nucleus respectively. The fluorescence images were captured using a Leica TCS SPE confocal microscope.

Table 1

Relationship of MSN-PLA grafting reaction time with combustible mass and average pore size.

Reaction time (h)	Combustible mass (%)	Average pore size (nm)
0	17.89	4.1000
3	32.03	3.3076
6	43.50	3.2868
24	42.90	2.9129
48	43.08	3.1041

2.7. *In vivo* wound healing and scar prevention study

Rabbit ear hypertrophic scar models were used for anti-scarring assessment of electrospun scaffolds. All studies were performed using New Zealand White Rabbits. Spherical biopsies were created on the surface of rabbit ears and covered with no treatment, pure PLA scaffolds and 20 mg and 50 mg/mL MSN-PLA-DOX scaffolds. Photographs of the wounds were taken every week over 8 weeks with rabbits sacrificed at week 4 and 8. During the experiment, no visible infection or extreme pain that hinders daily movement was observed in all rabbits. Wound healing assessment was performed by measuring the size of open wounds at varied time points. Hematoxylin and eosin (H&E) staining and Masson's Trichrome staining were performed for visualization of cutaneous tissues. Expression of Col-1, Col-3 and TGF- β 1 was quantified using qPCR of extracted scar tissues [19].

2.8. Statistical analysis

The data were presented as the mean \pm standard deviation (SD). Statistical differences were analyzed using one-way analysis of variance (ANOVA) followed by Tukey's multiple comparisons test (SPSS Statistics 17.0., IBM Corp., USA). p -value < 0.05 was considered statistically significant.

3. Results

Drug carriers designated for long-term applications require a spacious lumen to reserve ample quantities of molecules for passive release. This avoids the need to incorporate large amounts of carriers, which may cause clogging and interfere with the spinning dynamics during electrospinning. Despite the exceptional drug encapsulation ratio of MSNs, their highly porous nature imposes passive drug leakage through their exposed mesopores. Hence, to prevent excessive leakage upon contact with fluids, gatekeepers must be functionalized on the surface of MSNs in the hope of long-term release. PLA brushes were functionalized onto the surface of purchased MSN-COOH via a "graft from" method, which involved the ring-opening addition polymerization of lactides stemming from the surface of carboxylic acid groups, of which polymer brush length was controlled through reaction time. After the reaction, significant 1750 cm^{-1} peaks in all FTIR spectra of PLA groups signify the presence of C=O bonds of PLA and the successful chemical

functionalization (Fig. 2b). Additionally, the amount of PLA grafted onto the MSN surface was physically quantified to verify its role as a pore gatekeeper. TGA analysis displayed that the amount of combustible mass increased with reaction time up to 6 h, while the pore size quantified by BET decreased with reaction time up to 24 h (Table 1). XRD measurements further suggested that the crystallinity of MSNs was unaffected by the reaction conditions (Fig. S2). These results collectively suggested that the pore size of MSNs can be tunably reduced through the additive grafting of polymer brushes for delaying drug release.

The grafting of PLA, however, may potentially congest the mesopores and lead to vastly reduced drug encapsulation. Taking MSN-PLA at 24 h reaction as the balance between lowest pore size and shortest reaction duration of all MSNs, drug encapsulation efficiency was performed with model drug DOX owing to its small molecular size and high polarity. Studies have reported the self-assembly nature of DOX molecules onto highly charged nanocarriers owing to its innate carboxylic acid groups for positive charge adherence and amine groups for negative charge adherence. Thus DOX can be effectively assembled into the charged MSNs even through organic solvents. Drug loading using concentrated (50 mg/mL) DOX dissolved in HFIP extends the PLA brushes, and greatly increased the amount of encapsulated DOX of MSN-PLAs compared to their bare counterpart (~5 folds). Without gate-keepers, DOX molecules quickly diffused out of MSN-COOHs under washing with phosphate buffer saline (PBS) while the PLA brushes onto the surface of MSN-PLA pores collapse upon contact with aqueous environment and was able to retain significant amount of drug molecules in their lumen. Similar results were shown when the drug-loaded MSN-COOH and MSN-PLAs were dispersed in PBS for long-term release (Figs. 2e, S3). Without PLA brush gatekeepers, MSN-COOH exhibited significant burst release within 1 day and while MSN-PLA groups experienced no burst release and instead sustainably released only up to 5% of the encapsulated DOX over 90 days (Fig. S4). This demonstrates the long-term release potential of our nanocarriers under a controlled environment.

To ensure that the slowly releasing DOX retains its inhibitory effect against fibroblasts, 3T3 human fibroblasts was used as a preliminary cytotoxicity test for the nanocarriers. Indirect contact cytotoxicity in accordance with international standards for biomedical device 10,993-1 was performed to simulate the effect of encapsulating nanocarriers within a scaffold (Fig. 2e). At both 24 and 48 h after exposure to MSN-PLA-DOX infused medium, cell proliferation of 3T3s was significantly hindered even at dilution ratios up to 100x. This showed that the slow release of DOX and loading via HFIP did not hinder its ability to inhibit fibroblast activity, and the nanocarriers functioned under serum-based culture medium.

After establishment of anti-scarring agent nanocarriers, they require a bulk structure to achieve localized release and extension of drug diffusion distance. We electrospun core-shell PLA-ethanol/MSN fibers using pseudo-emulsion co-axial spinning to achieve stable dispensary of fibers (Fig. 1d). When dispersed in ethanol, MSN-PLA-DOX experienced minimal aggregation after sonication and the ethanol served both as barrier against external organic solvents for PLA (Fig. S1) and conduit for spinning owing to ethanol's low surface tension. Meanwhile, a high concentration PLA shell was anticipated to further increase the drug diffusion distance of DOX and diminish the water influx to the core MSNs. The formed fiber groups (10, 20, 50 mg/mL MSNs) were characterized using TEM and SEM after air drying (Figs. 3a, S5, 6). The hydrophobicity of the fiber groups was characterized using water contact angle assessment (Fig. S7). For all concentration groups, MSNs could be observed to be centered within the fiber lumen, but with vastly altered fiber morphologies owing to their occupied space within the fibers. 10 and 20 mg/mL groups had sparsely distributed MSNs throughout the fiber, with 20 mg/mL exhibiting thicker fiber diameters owing to the increased lumen size to accommodate the nanocarriers, while 50 mg/mL exhibited clusters of MSNs within the fiber lumen with the highest fiber diameter out of all groups. These varied morphologies also directly impact the mechanical properties of the electrospun scaffolds (Fig. 3c). Naturally, the higher the solute content of an electrospun fiber, the lower the tensile stress as nanocarriers create flaws in the fibers' cross sections. This was observed between the pure PLA, 10 and 20 mg/mL fiber groups. However, the clusters

of MSNs in the 50 mg/mL groups simultaneously enlarged the fiber size, causing an improvement in tensile modulus instead. Nevertheless, the tensile modulus of all fiber groups well exceeded the range of healed skin tissues, which supports the use of these scaffolds as wound dressings.

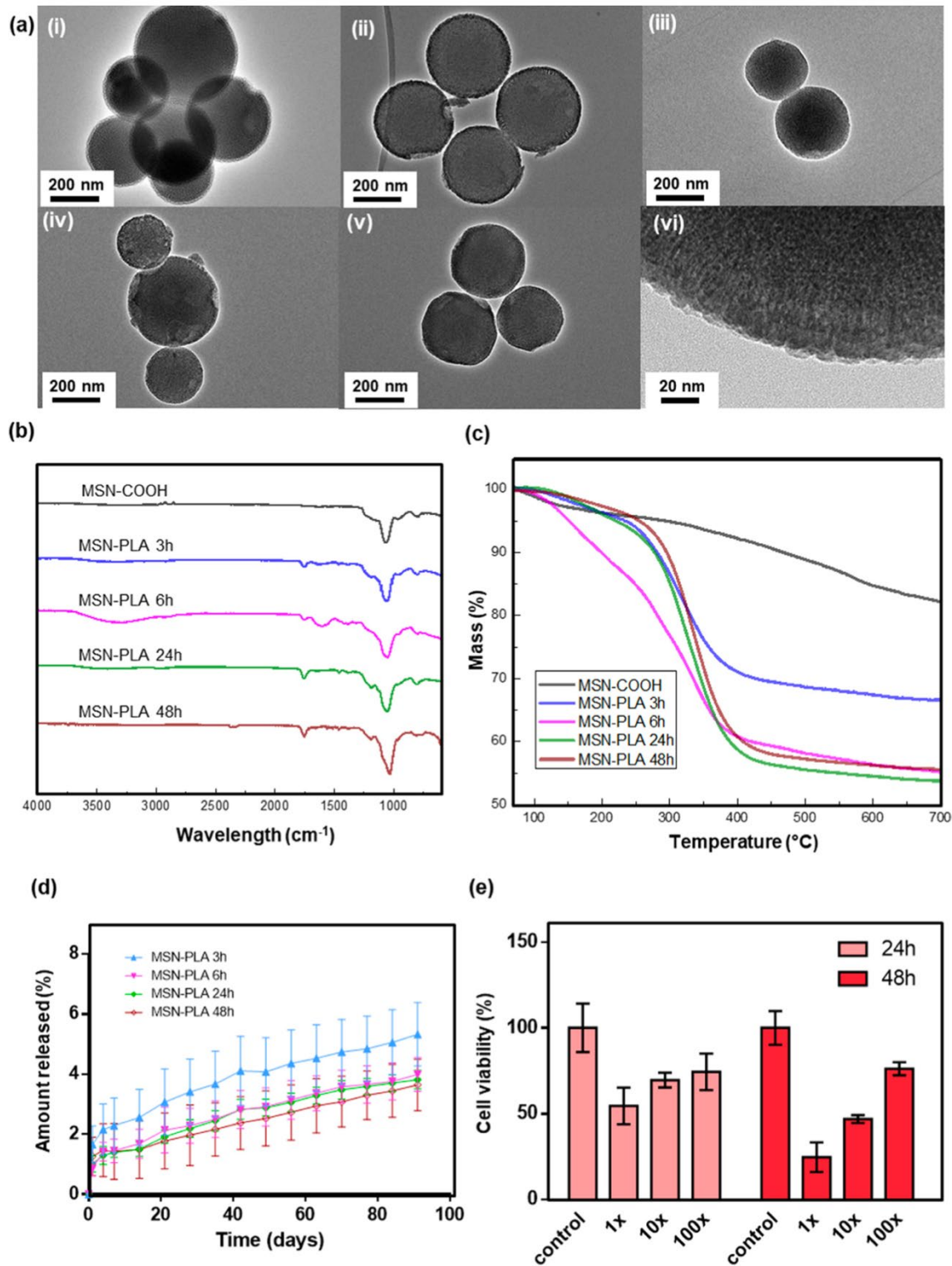


Fig. 2. Synthesis and characterization of MSN-PLAs. (a) TEM images of (i) MSN-COOH, (ii) MSN-PLA 3 h, (iii) MSN-PLA 6 h, (iv) MSN-PLA 24 h, (v) MSN-PLA 48 h, (vi) magnified view of MSN-PLA 24 h. (b) FTIR spectrum and (c) TGA analysis of MSN-PLAs of aforementioned reaction times. (d, e) MSN-PLA-DOX release profiles over 90 days and (f) cell inhibitory study via indirect contact 24 h and 48 h after addition of MSN-PLA-DOX co-cultured medium. Data were presented as mean \pm SD.

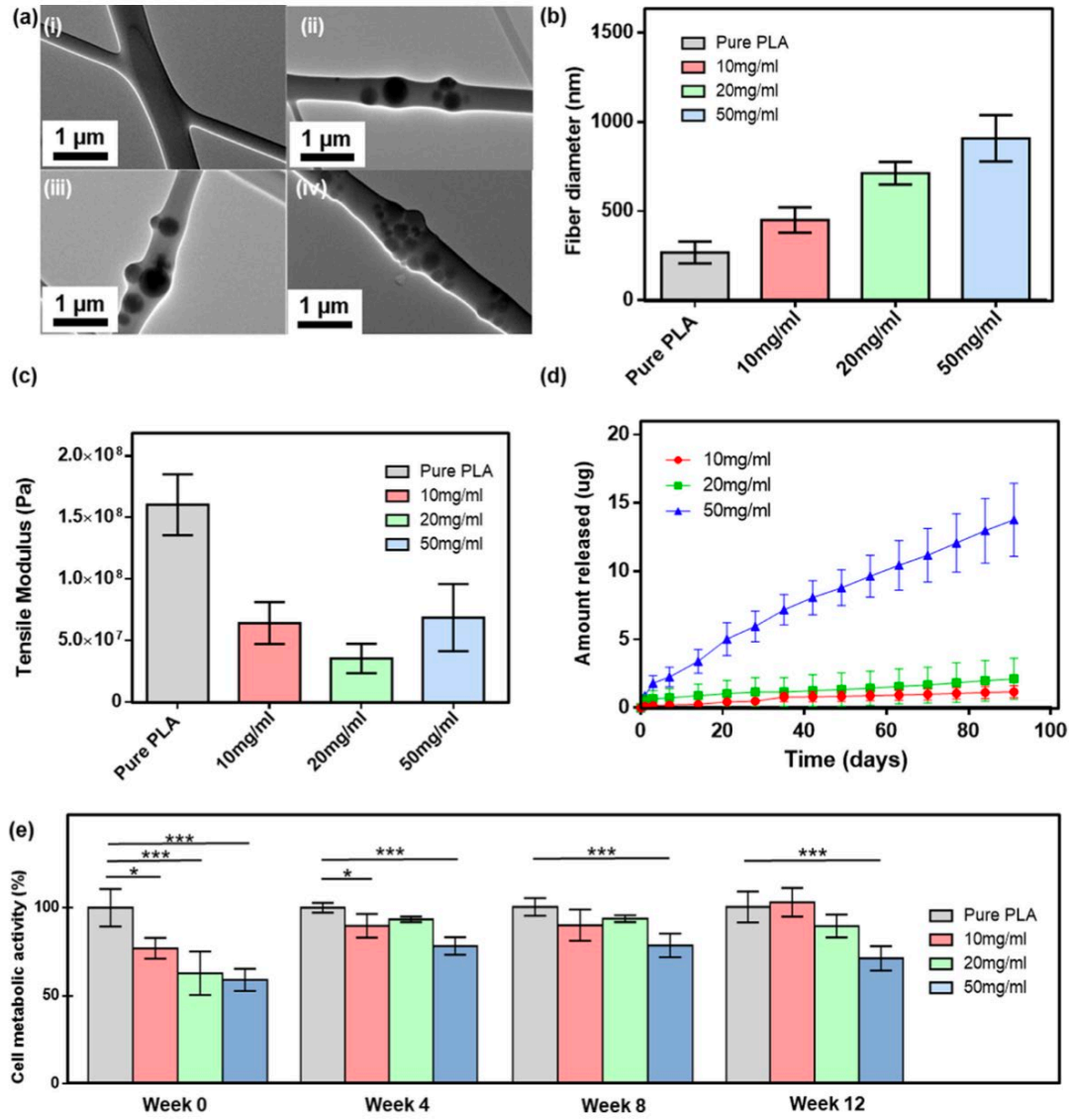


Fig. 3. Characterization of long-term drug release fibrous scaffolds. (a) TEM image, (b) average fiber diameter and (c) tensile modulus of fibrous scaffolds. After loading with DOX, (d) release profile and (e) fibroblast inhibitory study via indirect contact by introduction of membrane soaked medium. Data were presented as mean \pm SD and analyzed by one-way ANOVA ($n = 4$ for each sample, $*p < 0.05$, $**p < 0.01$, and $***p < 0.001$).

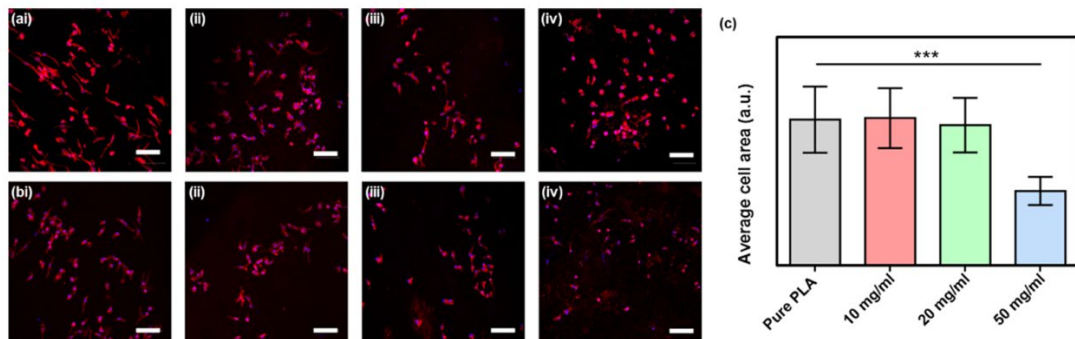


Fig. 4. Adhesion of 3T3 fibroblasts onto the fibrous scaffolds at (a) day 0 and (b) day 90 of the release study. (c) Quantification of cell spreading on the scaffolds for different MSN-PLA-DOX concentrations. Scale bar = 200 μ m. Data were presented as mean \pm SD and analyzed by one-way ANOVA ($n = 5$ for each sample, $*p < 0.05$, $**p < 0.01$, and $***p < 0.001$).

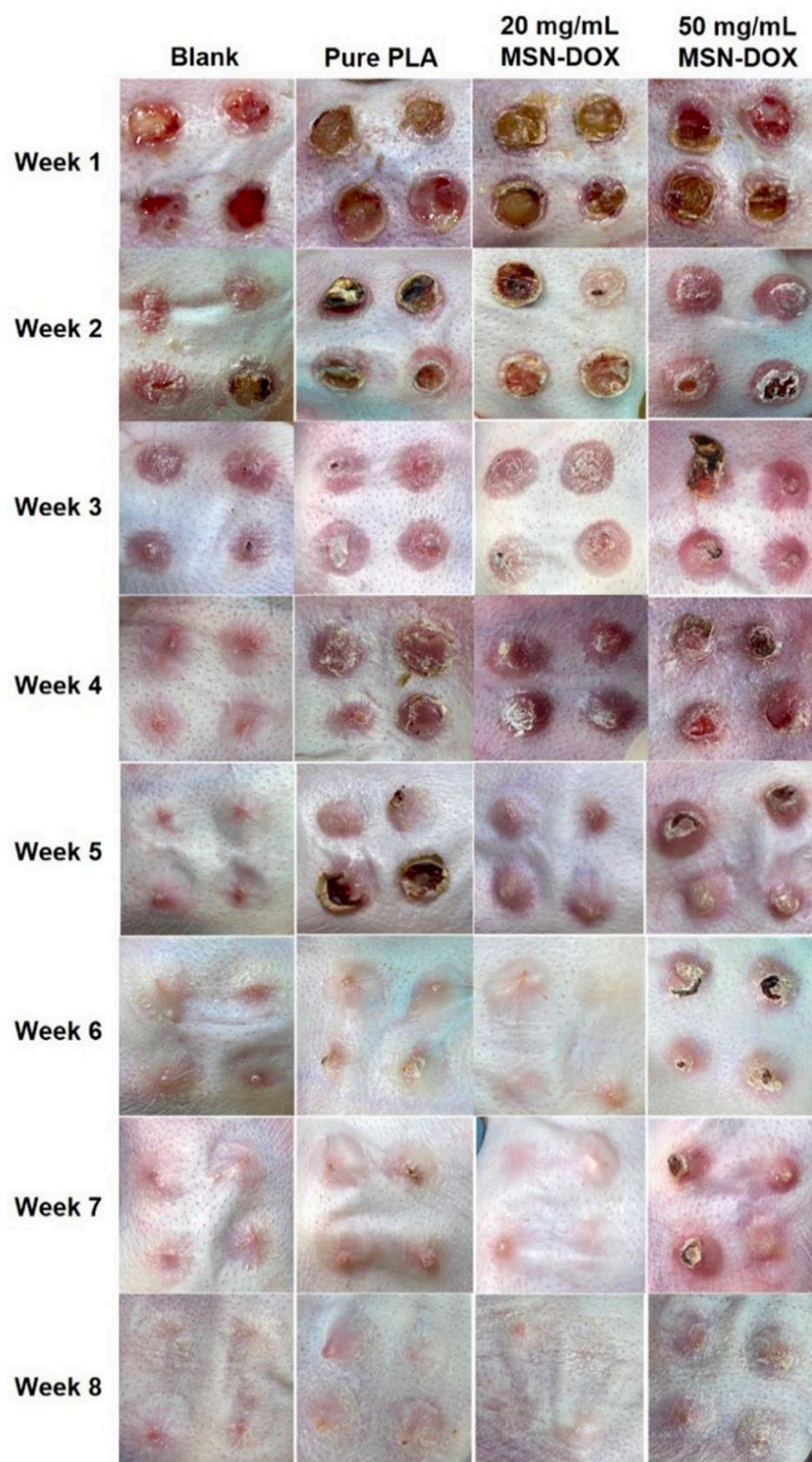


Fig. 5. Photographs of healing rabbit ears with no treatment (blank), treatment with pure PLA scaffolds, 20 and 50 mg/mL MSN-PLA-DOX scaffolds at set time points. Scale bar = 10 mm.

Despite the large differences in morphology, the drug release kinetics of all 3 MSN fiber groups remain similar presumably owing to the protection of carriers from contact from HFIP (Figs. 3d, S8). The absence of burst release from fibrous scaffolds also suggested the effectiveness of core-shell design on long-term

sustained release of encapsulated molecules (Fig. S9). Nevertheless, compared with the performance of nanocarriers alone, the lengthy spinning process and the brief, partial exposure of MSN-PLA-DOX to spinning solvents at the needle tip might have led to slight blending of DOX within the fiber shell, which could possibly create concerns for excessive initial inhibition of other cell types integral to wound healing. Thus, dosage control for this long-term release strategy is extremely important to ensure the complete healing of exposed wound beds. Preliminary dosage assessment was performed by indirect contact cytotoxicity assessment at designated time points over the average wound healing cycle (Fig. 3e). Varied inhibition was observed in all fiber groups compared with pure PLA control early, but differences became less significant for later time points except for 50 mg/mL groups. Additionally, adhesion assessment was performed to ensure that the cytotoxicity was controlled as fibroblast adhesion was vital to achieving wound closure and completing the wound cycle; the DOX concentration could not be oversaturated that it rendered native cells incapable of performing reparative functions. Actin staining displayed that all groups was able to support fibroblast adhesion (Fig. 4a,b). Notably, less cell spreading was observed in 50 mg/mL groups and the average cell size was quantified to be nearly half of other groups on both day 0 and day 90 (Fig. 4c). This shows that the inhibitory effect of our long-term release scaffolds was able to sustain beyond 90 days without majorly hindering the basic cellular functions of fibroblasts.

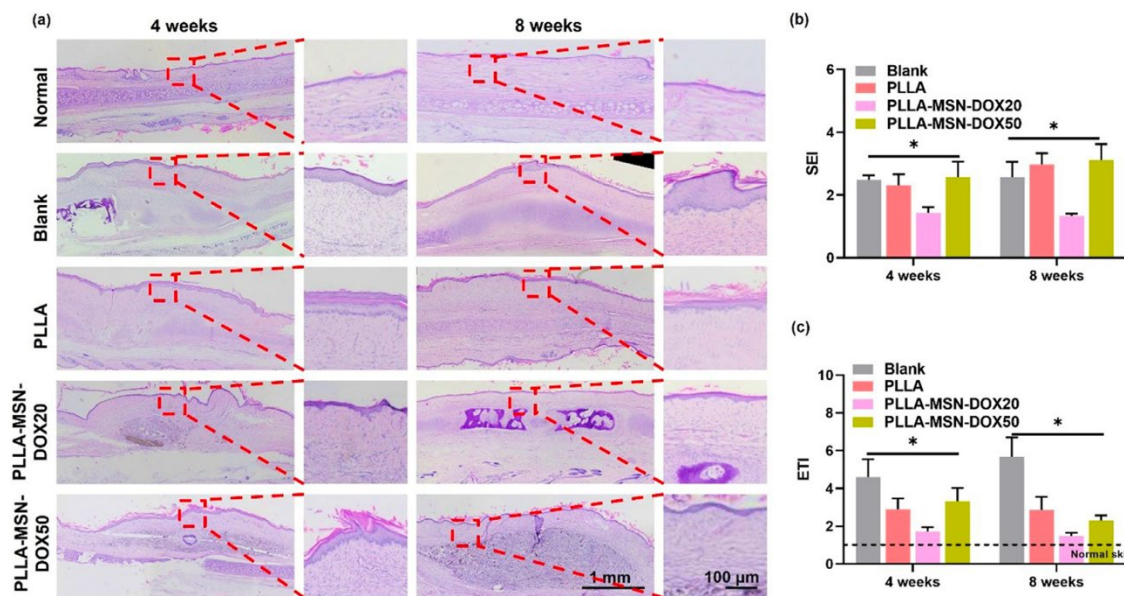


Fig. 6. (a) Hematoxylin and eosin staining of healing rabbit ear tissues. (b) Scar elevation index and (c) epidermal thickness index compared with surrounding tissues and normal skin respectively. Data were presented as mean \pm SD and analyzed by one-way ANOVA ($n = 3$ for each sample, $*p < 0.05$, $**p < 0.01$, and $***p < 0.001$).

With the promising results of in vitro dosage assessments, we have selected rabbit ear hypertrophic scar model for further assessment to establish the scaffold clinical relevancy, owing to its scarring reproducibility and responsiveness in an in vivo setting [20]. Circular wounds were created on the ears of New Zealand White Rabbits, and the wound bed was administered with no treatment and pure PLA scaffold as control, and 20 or 50 mg/mL group scaffolds as experimental groups. After 4 and 8 weeks, the rabbits were sacrificed for staining and quantification analysis. For all rabbit groups, wound closure was achieved with the 20 mg/mL group displaying the flattest healed tissues, while the 50 mg/mL group displayed a visible delay in the healing process (Figs. 5, S10). To verify our observations, we then quantified scar elevation index (SEI) and epidermal thickness index (ETI) in H&E stained samples, which showed that 20 mg/mL group exhibited both the lowest SEI and ETI, demonstrating the inhibition of granulation tissue formation and likeliness to healthy skin (Fig. 6a–c). In Masson's Trichrome stained scar tissues, both the 20 and 50 mg/mL groups exhibited reduced collagen deposition compared with the control PLA scaffolds (Fig. 7a,b). However, despite the effective inhibition of collagen formation, 50 mg/mL showed reduced anti-scarring efficacy in

terms of SEI and ETI compared with 20 mg/mL. The high drug concentration possibly induced hyperplasia in healing tissues and subsequently proliferation and thickening of the fibroblast layer, leading to raised scar tissues. These results suggest that only at certain dosages are long-term release scaffolds effective at inhibiting scar formation, and that the cautionary signs observed during the in vitro dosage assessment were amplified when performed on a living specimen with complex physiological microenvironments.

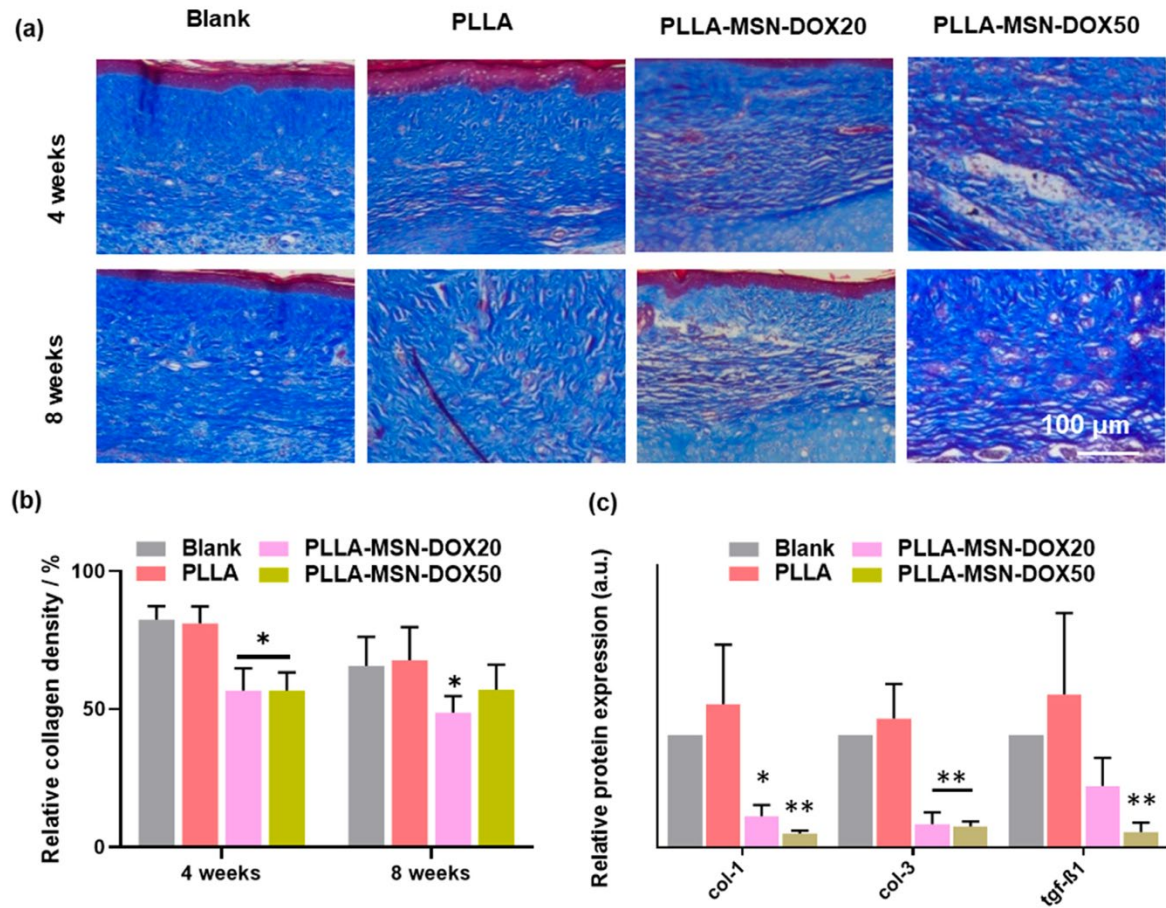


Fig. 7. (a) Masson's Trichrome staining images of healing rabbit ear tissues. Quantification of (b) relative collagen density and (c) expression of scar-related proteins by qPCR. Data were presented as mean \pm SD and analyzed by one-way ANOVA ($n = 3$ for each sample, * $p < 0.05$, ** $p < 0.01$, and *** $p < 0.001$).

To quantifiably assess the long-term treatment efficacy of our scaffolds, the expression of typical scar-associated genes collagen- I (Col-1), collagen-III (Col-3) and transforming growth factor beta 1 (TGF- β 1) was characterized using quantitative polymerase chain reaction (qPCR) (Fig. 7c). As reported, the reduced collagen synthesis can lead to improved scarring outcomes, and TGF- β 1 was the primary activator of collagen production in fibroblasts [21]. Thus, in recovering tissues less prone to scarring, lower expression of collagen I and III and TGF- β 1 should be observed. Significant reduction in expression levels for all 3 genes was observed for 20 and 50 mg/mL groups, suggesting the fundamental alteration of cellular activity at the healed tissues. Interestingly, an increase in scar-associated gene expression was observed for the pure PLA group, suggesting that the treatment of biologically inert electrospun fibers alone actually upregulated the activity and expression of these proteins. This has been reported by many studies that nanofibrous structures encourage the cell adhesion and proliferation to aid wound healing, and this suggested that the possible treatment without inhibitory molecules may also aggravate scar formation after wound closure [22]. Therefore, any treatment options prioritizing acceleration of wound healing should incorporate anti-scarring strategies in order to prevent subsequent scar formation. Particularly, long-term or staggered release of inhibitory agents from wound dressings will be vital to ensuring complete recovery of damaged tissues. In

this regard, the basal modulation of scar-associated genes suggests that the anti-scarring effect of our long-term release scaffolds could linger beyond the drug release profile within native cells and prevent a relapse of hypertrophic tissues.

4. Discussion

A wound dressing serves multiple purposes throughout the wound healing cycle. During the initial hemostasis phase, the dressing acts as a physical barrier to protect the vulnerable tissues from pathogens and infection. Chronic stimulation of endothelial cells by stretching was also reported to aggravate soft tissue scarring, thus a wound dressing ought to provide mechanical support to resist shear stress produced by day-to-day movement. Additionally, the dressing also doubles the role of the lost epidermis in retaining partial moisture, which is reported by many studies to facilitate wound healing. Hence, from a macroscopic perspective, wound dressings should display adequate strength, slow biodegradation and low pore size. Our drug delivery system scaffolds displayed 30–60 MPa while maintaining a nanofibrous structure gradual degradability, which provides a stable foundation for scab formation, cell adhesion, and mechanical support for wound recovery.

The physical properties of the long-term drug release fibrous scaffolds are all achieved while keeping the anti-scarring aspect of the wound dressing functional. While significant effort has been placed in scar prevention through improved wound healing, they could not fulfill the rigorous requirements of regulating trauma-induced tissue repair [23]. Up to 25% of loaded therapeutics dissipate upon first contact with fluids. The burst release of drug-encapsulated scaffolds greatly hindered their ability to support the entire wound healing cycle, while the lack of molecules of inhibitory nature showed the inability to fully circumvent scar formation. While the wound healing process was not fully complete within the study (16 days), the elevated levels of Col- I and III pose risks of scar formation during the remodeling phase [23]. On that front, our delivery system boasts two distinct release mechanic, diffusion- and degradation-based release of anti-scarring agents. Compared with studies which did not incorporate designs for extending drug diffusion distances, our scaffolds were able to retain most of its loaded drugs without activation over 90 days while the hydrogel-based scaffolds usually released 40% of its encapsulated therapeutics within 8–24 h [24]. The impact of the lack of long-term release was evident in the study design of *in vivo* characterization, where the scaffolds were replaced every two days. However, this potentially disturbs the wound bed and disrupts the healing process of skin tissues. To facilitate wound healing, it is preferable to avoid removal of dressing materials in the forms of a therapeutic reservoir for long-term release.

In our experiments, the PLA-MSN scaffolds were only applied once post-trauma without requirement for replacements throughout the entire wound healing cycle. The retention of bioactive agents was evident in rabbit hypertrophic models, where the scaffolds were able to support reduced scarring wound recovery over 8 weeks, and achieved exceptionally scar flatness and reduced collagen and TGF- β 1 expression. While efforts have been put in highly degradable electrospun scaffolds for repeated application, their fast degradability also greatly affects the local drug concentration and integrity of said scaffolds. Up to 50% of scaffolds' dry weight was lost upon immersion in proteases within 2 h, which greatly lowers the mechanical strength of the scaffolds, not to mention the burst release of anti-scarring agents within the short timeframe. While accelerated wound healing is displayed by the astragaloside IV (AS) loaded scaffolds applied to rat acute wound models, the lack of mechanical shielding may have attributed to the elevated amount of capillary formation, which is a widely reported risk factor for scar formation. Additionally, the effect of cellular activity modulation in terms of gene expression was largely insignificant between blank fibers and AS-loaded scaffolds during later stages of the wound healing process. Our scaffolds were able to achieve reduced collagen and TGF- β 1 expression 8 weeks post-trauma, showing a lasting reprogramming of cellular behaviours through the sustained release of anti-scarring agents.

All in all, the promising results of our long-term release fibrous drug delivery system grants it great potential in combination with other therapies to achieve extended therapeutic potential. Despite the favourable cell adhesion assessment results, however, PLA was only used as a proof-of-concept for the long-term release strategy owing to its widespread usage and experimentation, as well as general spinnability. Improved scaffold properties such as tissue adhesiveness could be further achieved by co-spinning various tissue adhesive bulk polymer solutions such as gelatin methacryloyl without altering the core concept of this study [25]. To achieve smart drug release, we can also modify our system to incorporate an enzyme-sensitive ligand on the surface of nanoparticles before grafting of PLA gatekeepers, which allows for minimal drug leakage and simultaneously activation of drug release when programmed conditions are met (cleaving of ligand by enzymes). In addition, the PLA gatekeepers could be substituted with positively charged polymers such as polyethylenimine to achieve gatekeeping and passive loading of negatively charged molecules. The non-rigorous requirements and simple mechanism of our long-term drug releasing electrospun fibrous scaffolds is also expected to possess high adaptability and translation into clinical application and solve other tissue engineering problems including inhibition of cancer development and tendon adhesion.

Data availability statement

The raw/processed data required to reproduce these findings cannot be shared at this time due to technical or time limitations.

Declaration of Competing Interest

The authors declare that they have no known competing financial interests or personal relationships that could have appeared to influence the work reported in this paper.

CRediT authorship contribution statement

Ho-Pan Bei: Conceptualization, Data curation, Formal analysis, Investigation, Methodology, Validation, Visualization, Writing – original draft, Writing – review & editing. **Tianpeng Xu:** Conceptualization, Data curation, Formal analysis, Investigation, Methodology, Validation, Visualization, Writing – original draft, Writing – review & editing. **Jing Zhou:** Data curation, Formal analysis, Investigation, Methodology, Validation, Visualization, Writing – review & editing. **Zhifei Dong:** Data curation, Formal analysis, Investigation, Methodology, Validation, Visualization, Writing – review & editing. **Yufeng Wang:** Data curation, Formal analysis, Investigation, Methodology, Validation, Visualization, Writing – review & editing. **Kak Yuen Wong:** Conceptualization, Funding acquisition, Investigation, Project administration, Resources, Supervision, Validation, Writing – review & editing. **Huaiyu Wang:** Conceptualization, Funding acquisition, Investigation, Project administration, Resources, Supervision, Validation, Writing – review & editing. **Xin Zhao:** Conceptualization, Funding acquisition, Investigation, Project administration, Resources, Supervision, Validation, Writing – original draft, Writing – review & editing.

This work was supported by the Early Career Scheme (25208218) of the Research Grants Council of Hong Kong.

Supplementary materials

Supplementary material associated with this article can be found, in the online version, at doi:10.1016/j.apmt.2022.101463.

References

- [1] J.C. Schneider, R. Holavanahalli, P. Helm, R. Goldstein, K. Kowalske, Contractions in burn injury: defining the problem, *J. burn care Res.* 27 (2006) 508–514.
- [2] E. Shirakami, S. Yamakawa, K. Hayashida, Strategies to prevent hypertrophic scar formation: a review of therapeutic interventions based on molecular evidence, *Burns Trauma* 8 (2020), doi:10.1093/burnst/tkz003.
- [3] T.H. Kim, Y. Jung, S.H. Kim, Nanofibrous electrospun heart decellularized extracellular matrix-based hybrid scaffold as wound dressing for reducing scarring in wound healing, *Tissue Eng. Part A* 24 (2018) 830–848.
- [4] B.O.O. Boni, L. Lamboni, B.M. Bakadia, S.A. Hussein, G. Yang, Combining silk sericin and surface micropatterns in bacterial cellulose dressings to control fibrosis and enhance wound healing, *Eng. Sci.* 10 (2020) 68–77.
- [5] S. Liu, G. Wu, X. Zhang, J. Yu, M. Liu, Y. Zhang, P. Wang, X. Yin, Degradation and drug-release behavior of polylactic acid (PLA) medical suture coating with tea polyphenol (TP)-polycaprolactone (PCL)/polyglycolide (PGA), *Fibers Polym.* 20 (2019) 229–235.
- [6] M.M. Coppola, R. Salzillo, F. Segreto, P. Persichetti, Triamcinolone acetonide intralesional injection for the treatment of keloid scars: patient selection and perspectives, *Clin. Cosmet. Investig. Dermatol.* 11 (2018) 387.
- [7] V.K. Pandey, G. Ajmal, S.N. Upadhyay, P.K. Mishra, Nano-fibrous scaffold with curcumin for anti-scar wound healing, *Int. J. Pharm.* 589 (2020) 119858.
- [8] M. Séon-Lutz, A.C. Couffin, S. Vignoud, G. Schlatter, A. Hébraud, Electrospinning in water and in situ crosslinking of hyaluronic acid/cyclodextrin nanofibers: towards wound dressing with controlled drug release, *Carbohydr. Polym.* 207 (2019) 276–287.
- [9] X. Zhao, X. Sun, L. Yildirim, Q. Lang, Z.Y.W. Lin, R. Zheng, Y. Zhang, W. Cui, N. Annabi, A. Khademhosseini, Cell infiltrative hydrogel fibrous scaffolds for accelerated wound healing, *Acta Biomater.* 49 (2017) 66–77.
- [10] X. Sun, Q. Lang, H. Zhang, L. Cheng, Y. Zhang, G. Pan, X. Zhao, H. Yang, Y. Zhang, H.A. Santos, Electrospun photocrosslinkable hydrogel fibrous scaffolds for rapid in vivo vascularized skin flap regeneration, *Adv. Funct. Mater.* 27 (2017) 1604617.
- [11] F. Aavani, S. Khorshidi, A. Karkhaneh, A concise review on drug-loaded electrospun nanofibres as promising wound dressings, *J. Med. Eng. Technol.* 43 (2019) 38–47.
- [12] R.S. Ambekar, B. Kandasubramanian, Advancements in nanofibers for wound dressing: a review, *Eur. Polym. J.* 117 (2019) 304–336.
- [13] X. Zhao, S. Jiang, S. Liu, S. Chen, Z.Y.W. Lin, G. Pan, F. He, F. Li, C. Fan, W. Cui, Optimization of intrinsic and extrinsic tendon healing through controllable water-soluble mitomycin-C release from electrospun fibers by mediating adhesion-related gene expression, *Biomaterials* 61 (2015) 61–74.
- [14] S. Jiang, X. Zhao, S. Chen, G. Pan, J. Song, N. He, F. Li, W. Cui, C. Fan, Down-regulating ERK1/2 and SMAD2/3 phosphorylation by physical barrier of celecoxib-loaded electrospun fibrous membranes prevents tendon adhesions, *Biomaterials* 35 (2014) 9920–9929.
- [15] M. Manzano, M. Vallet-Regí, Mesoporous silica nanoparticles for drug delivery, *Adv. Funct. Mater.* 30 (2020) 1902634.
- [16] L. Zhang, H.P. Bei, Y. Piao, Y. Wang, M. Yang, X. Zhao, Polymer-brush-grafted mesoporous silica nanoparticles for triggered drug delivery, *ChemPhysChem* 19 (2018) 1956–1964.
- [17] X. Zhao, C. Hu, G. Pan, W. Cui, Pomegranate-structured electrosprayed microspheres for long-term controlled drug release, *Part. Part. Syst. Charact.* 32 (2015) 529–535.
- [18] L. Wei, N. Hu, Y. Zhang, Synthesis of polymer—mesoporous silica nanocomposites, *Materials (Basel)* 3 (2010) 4066–4079.
- [19] M. Gholipourmalekabadi, S. Khosravimelal, Z. Nokhbedehghan, M. Sameni, V. Jajarmi, A.M. Urbanska, H. Mirzaei, M. Salimi, N.P.S. Chauhan, M. Moobaraki, Modulation of hypertrophic scar formation using amniotic membrane/electrospun silk fibroin bilayer membrane in a rabbit ear model, *ACS Biomater. Sci. Eng.* 5 (2019) 1487–1496.

- [20] J. Zhang, Y. Li, X. Bai, J. Shi, D. Hu, Recent advances in hypertrophic scar, *Histol. Histopathol.* 33 (2017) 27–39.
- [21] L. Nabai, A. Pourghadiri, A. Ghahary, Hypertrophic scarring: current knowledge of predisposing factors, cellular and molecular mechanisms, *J. Burn Care Res.* 41 (2020) 48–56.
- [22] E. Vatankhah, M.P. Prabhakaran, G. Jin, L.G. Mobarakeh, S. Ramakrishna, Development of nanofibrous cellulose acetate/gelatin skin substitutes for variety wound treatment applications, *J. Biomater. Appl.* 28 (2014) 909–921.
- [23] X. Guo, Y. Liu, H. Bera, H. Zhang, Y. Chen, D. Cun, V. Foderà, M. Yang, α -Lactalbumin-based nanofiber dressings improve burn wound healing and reduce scarring, *ACS Appl. Mater. Interfaces* 12 (2020) 45702–45713.
- [24] L. Zhang, Y. Tai, X. Liu, Y. Liu, Y. Dong, Y. Liu, C. Yang, D. Kong, C. Qi, S. Wang, Natural polymeric and peptide-loaded composite wound dressings for scar prevention, *Appl. Mater. Today* 25 (2021) 101186.
- [25] Y. Yang, T. Xu, Q. Zhang, Y. Piao, H.P. Bei, X. Zhao, Biomimetic, stiff and adhesive periosteum with osteogenic angiogenic coupling effect for bone regeneration, *Small* 17 (2021) 2006598.